Supporting Information for the manuscript

Structure calculation from unambiguous long-range amide and methyl ^{1}H-^{1}H distance restraints for a micro-crystalline protein with MAS solid-state NMR spectroscopy

by

Rasmus Linser, Benjamin Bardiaux, Victoria Higman, Uwe Fink, and Bernd Reif

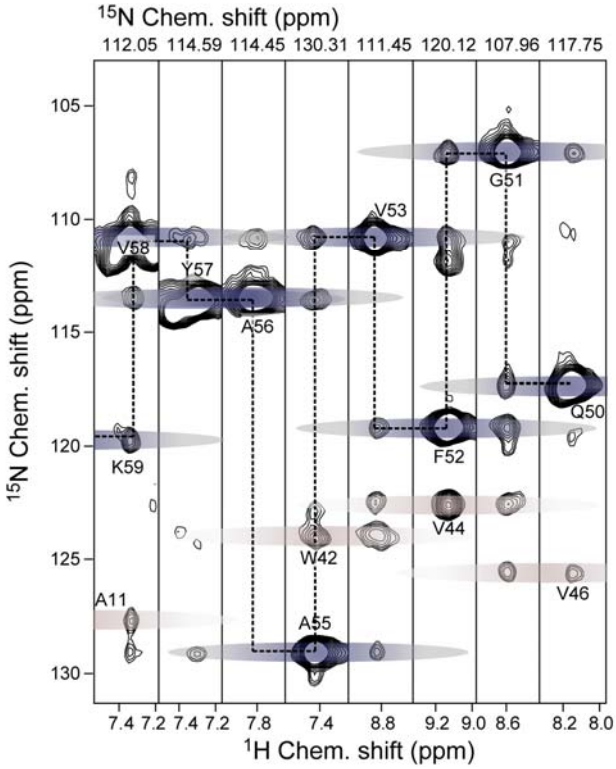

Supplementary Figure 1. Sequential walk from a 3D N··N,H RFDR correlation experiment. The correlations are solely based on ^{1}H and ^{15}N chemical shifts and can assist sequential assignments when ^{13}C based backbone experiments do not yield unambiguous assignments. In addition to sequential correlation (blue), non-sequential contacts (e.g. across the beta-strand) are observed (red). The 3D experiment was recorded within 4 h employing a RFDR mixing time of 8 ms, setting t_1^{max} (^{15}N) = 20 ms.

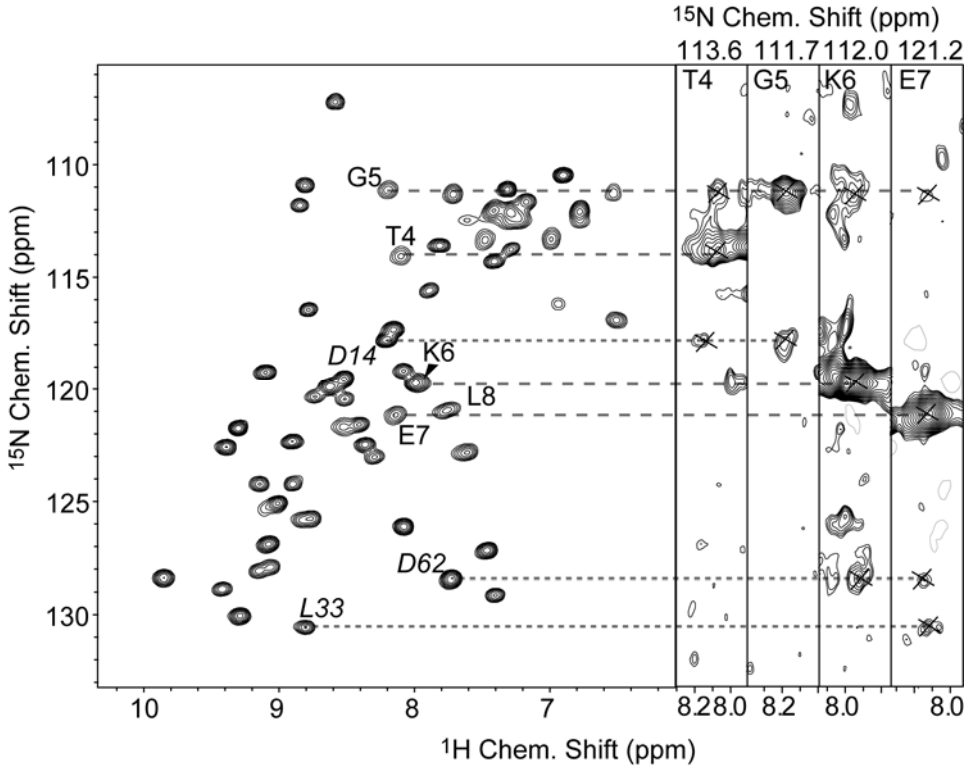

Supplementary Figure 2. Sequential walk for dynamic residues in the N-terminus (using the pulse scheme represented in Figure 1C of the main manuscript). The experiment confirms TROSY based assignments in the N-terminus of α-spectrin SH3.[1] The experiment was recorded in 4 h employing a RFDR mixing time of 8 ms.

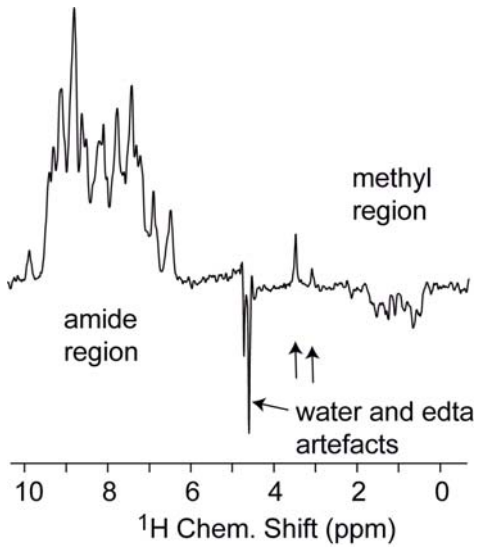

Supplementary Figure 3. First increment of a time-shared 3D H··N/C,H correlation experiment (pulse scheme represented in Figure 1F of the main manuscript). The spectrum was recorded using 8 scans. The experimental time for each increment amounts to ca. 2 s. The CP transfer time was restricted to 1000 μs to suppress long-range $^{1}H^{N}/^{13}C^{\alpha}$ transfers.

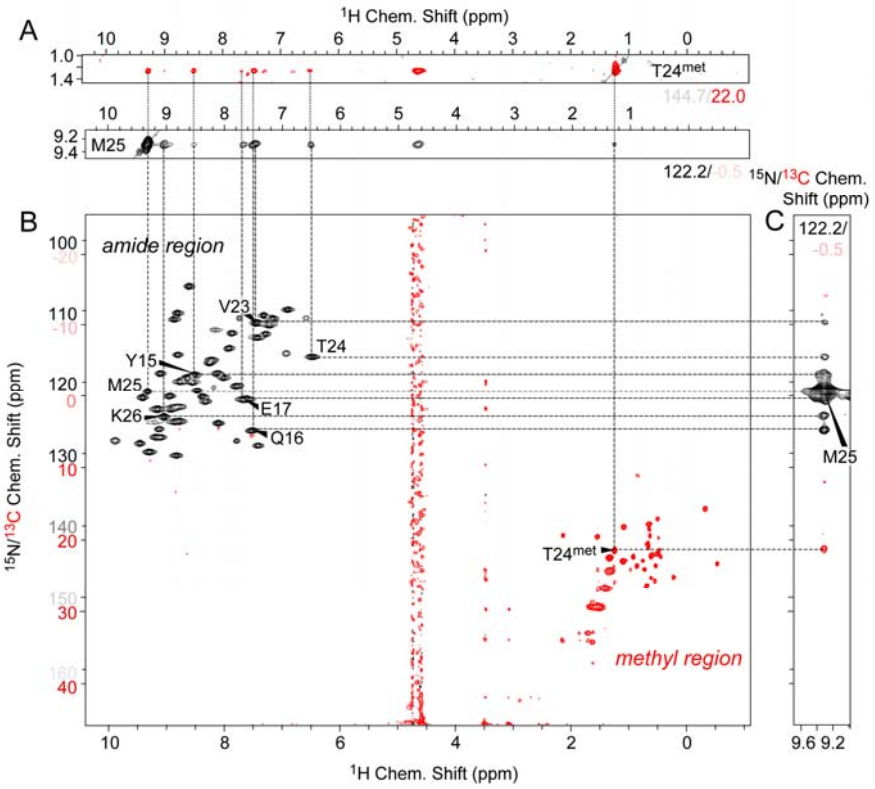

Supplementary Figure 4. Complementary time-shared 3D experiments with synchronous ^{13}C and ^{15}N evolution periods (as in Figure 4 of the main manuscript, but displaying the full ^{1}H spectral window). Artifacts in B) at ^{1}H chemical shifts of 4.6, 3.5, and 3.0 ppm are due to insufficient water suppression and $[Cu(edta)]^{2-}$. Cross peaks at the water resonance frequency can be attributed to correlations between amide and exchanging hydroxyl protons which exchange rapidly with water.[2]

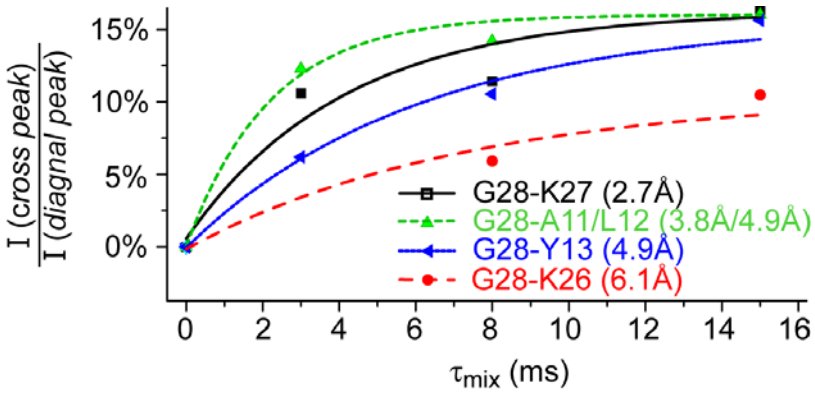

Supplementary Figure 5. Buildup of cross peak intensity for G28 as a function of the RFDR mixing time τ_{mix}. Data was extracted from the 3D N··N,H spectra. Intensities found for different τ_{mix} are scaled with respect to the intensity of the diagonal peak of G28 in each case in order to correct for pulse imperfections during RFDR mixing. Neither T_1 decay in general nor differential T_1 decay during τ_{mix} is expected to be significant for these

short mixing times.[3] Cross peak intensities reach a plateau at long mixing times due to spin diffusion. Data have been fit using a mono-exponential function in order to guide the eye and aid identification of suitable experimental mixing times. A quantitative analysis of the data is beyond the focus of the manuscript. In contrast, for our structure calculation we employed two independent spectra (with 3 and 8 ms mixing) with different upper distance values (see main manuscript for a description of the transformation from intensities to distances). This approach is in agreement with Zhou et al.[4] and allows fast data acquisition.

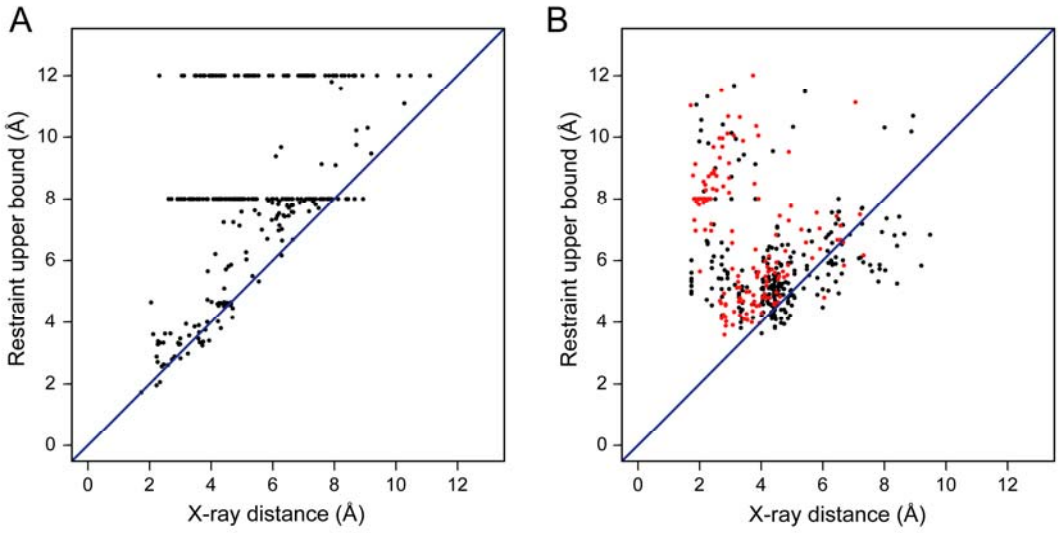

Supplementary Figure 6. **A**) Correlation between the upper bound of the manually assigned distance restraints and the corresponding distances in the X-ray structure. The restraint upper bounds derived from the manual assignments and TALOS+ match the "real" (i. e. X-ray) distances reasonably well. Restraint upper bounds are obtained following the protocol described in "Structure calculation from unambiguous manual assignments" in the Experimental Section of the main manuscript. **B**) Correlation for the automated calculation. Restraints were obtained from ambiguous data, using only the proton chemical shift encoded H··C/N,H correlations. The data points represent the restraints obtained by ARIA in the final assignment iteration. Despite the poor correlation obtained in the iterative automated assignment, a very high correlation between X-ray and NMR structure is achieved in the later stage of the structure calculation procedure (backbone RMSD of 1.6 Å). "Restraint upper bounds" refers to the distance extracted from the cross peak intensities according to Eq. (1) and (2) in the main manuscript. Restraints containing a single assignment possibility at the end of the automated procedure (unambiguous) are shown in black, whereas restraints that remain ambiguous are in red. "X-ray distance" denotes the ^{1}H,^{1}H distance in accordance with the cross peak assignment and can therefore differ in A) and B).

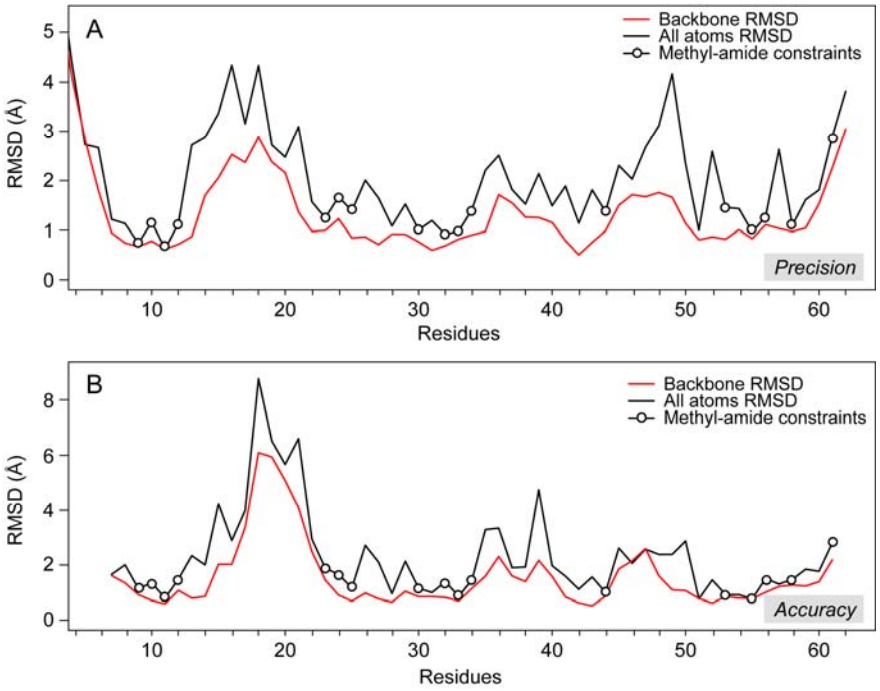

Supplementary Figure 7. Precision (**A**) and accuracy, i.e. deviation from the X-ray structure 2NUZ, (**B**) as a function of residue. The red and black curves refer to the backbone and all atoms RMSD, respectively. Circles denote the residues for which methyl-amide distance restraints were available

Simulated annealing protocols for structure calculation

All structure calculations were performed in CNS[5] with the standard molecular dynamics simulated annealing (SA) protocols implemented in ARIA.[6,7] Except for the number of molecular dynamics steps, all parameters were set to their default values. The lengths of the different SA stages used in the 3 calculations performed are listed in Supplementary Table 1. In each case, a randomized structure served as a starting conformation for the SA. For the calculation with dihedral angle restraints alone, only the SA stages in torsion angle space were accomplished. The calculation applying manually assigned unambiguous distance restraints corresponded to a single ARIA iteration. The automated calculation from ambiguous unassigned cross peaks was performed in ARIA 2.3, using 9 iterations (100 structures calculated per iteration).

The total computational times (using 20 processors) were: (i) 21 min for the calculation with TALOS+ derived restraints, (ii) 139 min for the unambiguous restraints and (iii) 175 min for the complete ARIA procedure from unassigned cross peaks.

Supplementary Table 1: Number of molecular dynamics steps in the simulated annealing protocol employed for the different calculations. As a result of the longer time-step employed in TAD (Torsion Angle Dynamics) (27 fs), the effective length of the TAD phases is actually 9x shorter. For the sake of consistency, the lengths of the different phases are here expressed in number of Cartesian MD steps.

Type of MD	**SA phase**	**TALOS+ restraints only**	**manual**	**automated**
Torsion	high Temp.	20000	50000	20000
	cooling 1	100000	120000	50000
Cartesian	cooling 1	-	120000	50000
	cooling 2	-	96000	40000

Supplementary Table 2: Distance values from distance restraints among amide protons and between amide and methyl protons in the structure calculation from unambiguous manual assignments.

Residue 1	Atom 1	Residue 2	Atom 2	Upper distance (Å)	X-ray distance (Å)	Mixing time (ms)
8	HN	33	HN	8.0	4.8	3
8	HN	61	HN	8.0	4.1	3
9	HN	8	HN	4.6	4.5	3
9	HN	9	HG1#	3.3	3.0	3
9	HN	11	HN	7.0	6.2	3
9	HN	31	HN	8.0	3.0	3
9	HN	32	HN	8.0	5.0	3
10	HN	9	HG2#	3.5	3.6	3
10	HN	10	HD1#	3.8	4.3	3
10	HN	10	HD2#	4.0	4.2	3
10	HN	29	HN	8.0	8.1	3
10	HN	30	HD1#	8.0	4.5	3
10	HN	31	HN	8.0	4.9	3
10	HN	58	HN	8.0	6.9	3
10	HN	59	HN	8.0	2.6	3
10	HN	61	HN	8.0	4.4	3
11	HN	10	HN	4.5	4.5	3
11	HN	13	HN	6.7	5.8	3
11	HN	28	HN	8.0	3.8	3

11	HN	29	HN	8.0	3.7	3
11	HN	30	HN	8.0	5.0	3
11	HN	31	HN	8.0	4.2	3
11	HN	59	HN	8.0	5.0	3
12	HN	12	HD2#	3.9	3.5	3
12	HN	13	HN	2.6	2.4	3
12	HN	28	HN	8.0	4.9	3
12	HN	57	HN	8.0	6.0	3
12	HN	58	HG1#	8.0	3.4	3
12	HN	58	HN	8.0	4.6	3
12	HN	59	HN	8.0	4.3	3
13	HN	14	HN	4.6	4.4	3
13	HN	15	HN	7.9	6.2	3
13	HN	27	HN	8.0	5.4	3
13	HN	28	HN	8.0	4.9	3
13	HN	29	HN	8.0	6.4	3
13	HN	58	HN	8.0	6.0	3
14	HN	15	HN	4.6	4.6	3
14	HN	27	HN	8.0	3.3	3
15	HN	16	HN	4.7	4.0	3
15	HN	25	HN	8.0	2.9	3
15	HN	26	HN	8.0	5.0	3
15	HN	27	HN	8.0	4.7	3
16	HN	16	HE21	6.7	6.6	3
16	HN	25	HN	8.0	5.0	3
17	HN	15	HN	7.4	6.1	3
17	HN	24	HN	8.0	4.1	3
17	HN	25	HN	8.0	4.7	3
18	HN	16	HN	7.7	6.5	3
18	HN	19	HN	4.6	2.0	3
18	HN	22	HN	8.0	4.8	3
19	HN	17	HN	7.9	5.9	3
19	HN	22	HN	8.0	3.5	3
19	HN	23	HN	8.0	6.0	3
19	HN	24	HN	8.0	7.8	3
22	HN	51	HN	8.0	7.9	3
22	HN	52	HN	8.0	4.3	3
23	HN	23	HG1#	3.3	2.3	3
23	HN	24	HN	4.5	4.4	3
23	HN	25	HN	7.4	6.4	3
23	HN	44	HN	8.0	6.1	3
23	HN	51	HN	8.0	5.4	3
23	HN	52	HN	8.0	3.3	3
23	HN	53	HN	8.0	4.9	3
24	HN	25	HN	4.6	4.5	3
25	HN	14	HN	8.0	7.4	3
25	HN	24	HG2#	3.6	2.5	3
25	HN	26	HN	4.6	4.4	3

25	HN	27	HN	7.8	6.6	3
26	HN	13	HN	8.0	7.5	3
26	HN	24	HG2#	5.7	4.5	3
26	HN	29	HN	8.0	4.3	3
27	HN	29	HN	8.0	4.7	3
28	HN	14	HN	8.0	6.3	3
30	HN	31	HN	4.6	4.3	3
31	HN	9	HG1#	8.0	5.0	3
31	HN	29	HN	7.6	6.6	3
31	HN	30	HD1#	4.7	3.9	3
31	HN	30	HG2#	3.5	3.0	3
31	HN	32	HN	4.6	4.5	3
31	HN	33	HN	7.5	6.2	3
32	HN	11	HN	8.0	8.4	3
32	HN	44	HN	8.0	7.4	3
32	HN	45	HN	8.0	3.1	3
32	HN	46	HN	8.0	5.2	3
33	HN	32	HG2#	3.6	2.7	3
33	HN	32	HN	4.6	4.5	3
33	HN	34	HD1#	6.2	6.3	3
34	HN	7	HN	8.0	7.8	3
34	HN	8	HN	8.0	8.9	3
34	HN	34	HD1#	3.7	3.8	3
34	HN	34	HD2#	3.9	3.6	3
34	HN	42	HN	8.0	7.9	3
34	HN	44	HN	8.0	4.6	3
35	HN	42	HN	8.0	7.2	3
35	HN	43	HN	8.0	3.1	3
35	HN	44	HN	8.0	5.2	3
38	HD21	39	HN	6.2	4.1	3
38	HD21	40	HN	7.2	4.7	3
38	HD21	41	HN	7.6	5.0	3
38	HD21	42	HE1	8.0	7.7	3
38	HD21	42	HN	8.0	8.4	3
39	HN	40	HN	2.6	2.5	3
39	HN	42	HE1	8.0	5.1	3
40	HN	41	HN	2.7	2.3	3
40	HN	42	HE1	8.0	5.0	3
40	HN	42	HN	7.0	6.3	3
41	HE1	42	HN	7.7	7.5	3
41	HN	42	HE1	8.0	4.9	3
41	HN	42	HN	4.5	4.2	3
41	HN	55	HN	8.0	4.2	3
41	HN	56	HN	8.0	6.5	3
42	HE1	35	HN	8.0	7.8	3
42	HN	53	HN	8.0	3.1	3
42	HN	55	HN	8.0	3.4	3
43	HN	42	HN	4.5	4.5	3

43	HN	44	HN	4.6	4.5	3
44	HN	34	HD1#	8.0	3.6	3
44	HN	50	HN	8.0	7.1	3
44	HN	51	HN	8.0	2.7	3
44	HN	52	HN	8.0	4.9	3
44	HN	53	HN	8.0	4.3	3
45	HN	44	HG1#	3.3	3.6	3
45	HN	44	HN	4.5	4.4	3
46	HN	44	HN	7.3	6.1	3
46	HN	49	HN	8.0	3.4	3
46	HN	50	HE22	8.0	7.6	3
46	HN	50	HN	8.0	4.9	3
46	HN	52	HN	8.0	8.7	3
49	HN	47	HD22	8.0	7.2	3
49	HN	50	HE22	8.0	7.8	3
49	HN	50	HN	4.7	4.4	3
49	HN	51	HN	7.9	7.0	3
50	HE21	50	HE22	1.7	1.7	3
50	HN	50	HE22	7.4	6.5	3
50	HN	51	HN	4.6	4.4	3
51	HN	23	HG1#	8.0	3.0	3
51	HN	34	HD1#	8.0	3.6	3
51	HN	46	HN	8.0	4.9	3
51	HN	52	HN	4.6	4.3	3
51	HN	53	HN	7.9	6.0	3
52	HN	53	HN	4.6	4.5	3
53	HN	53	HG1#	3.3	2.9	3
55	HN	40	HN	8.0	5.5	3
55	HN	42	HE1	8.0	5.8	3
55	HN	43	HN	8.0	7.7	3
55	HN	56	HN	2.9	2.8	3
56	HN	57	HN	2.8	2.7	3
57	HN	42	HN	8.0	6.5	3
58	HN	56	HN	7.2	4.4	3
58	HN	58	HG#	2.1	2.3	3
58	HN	59	HN	4.6	4.4	3
59	HN	12	HD2#	8.0	3.9	3
59	HN	13	HN	8.0	6.6	3
59	HN	31	HN	8.0	6.6	3
59	HN	60	HN	4.6	4.2	3
59	HN	61	HN	7.8	6.2	3
60	HN	10	HN	8.0	4.8	3
60	HN	61	HN	4.6	4.6	3
61	HN	9	HG2#	8.0	5.3	3
61	HN	9	HN	8.0	4.9	3
61	HN	10	HD1#	8.0	7.3	3
61	HN	10	HD2#	8.0	6.8	3
61	HN	61	HD1#	4.0	3.9	3

7	HN	33	HN	12.0	4.9	8
8	HN	60	HN	12.0	8.2	8
9	HN	9	HG2#	3.4	2.3	8
9	HN	12	HN	10.3	9.1	8
9	HN	30	HN	12.0	7.0	8
9	HG1#	59	HN	12.0	4.2	8
9	HG2#	60	HN	12.0	5.5	8
11	HN	10	HD2#	4.5	4.7	8
11	HB#	12	HN	3.0	3.2	8
11	HN	30	HD1#	12.0	3.8	8
11	HN	58	HN	12.0	7.7	8
11	HN	61	HN	12.0	8.7	8
12	HN	10	HD2#	6.3	5.1	8
12	HN	12	HD1#	3.7	3.6	8
12	HN	58	HG2#	12.0	5.2	8
12	HD1#	59	HN	12.0	4.0	8
13	HN	11	HB#	3.9	3.2	8
13	HN	12	HD2#	4.2	4.7	8
13	HN	25	HN	12.0	8.0	8
13	HN	57	HN	12.0	6.5	8
14	HN	16	HN	7.6	7.2	8
14	HN	24	HG2#	12.0	7.3	8
15	HN	16	HE21	9.5	9.2	8
15	HN	24	HG2#	12.0	3.7	8
15	HN	53	HG2#	12.0	6.9	8
16	HE21	16	HE22	1.7	1.7	8
17	HN	16	HE22	8.0	6.3	8
17	HN	52	HN	12.0	8.7	8
18	HN	24	HG2#	12.0	7.1	8
22	HN	25	HN	11.1	10.3	8
23	HN	23	HG2#	3.4	3.9	8
23	HG1#	46	HN	12.0	4.1	8
23	HG2#	46	HN	12.0	3.5	8
24	HG2#	16	HN	12.0	4.3	8
24	HN	23	HG2#	3.6	2.1	8
24	HN	24	HG2#	3.4	3.7	8
25	HE#	13	HN	12.0	3.1	8
25	HE#	25	HN	5.1	4.4	8
25	HE#	26	HN	5.3	5.5	8
25	HE#	58	HN	12.0	4.3	8
26	HN	11	HB#	12.0	3.9	8
26	HN	14	HN	12.0	7.1	8
26	HN	16	HN	12.0	8.6	8
26	HN	30	HD1#	11.6	8.2	8
26	HN	31	HN	12.0	8.3	8
26	HN	49	HN	12.0	10.5	8
26	HN	53	HG1#	12.0	6.4	8
27	HN	11	HB#	12.0	4.1	8

28	HN	10	HD2#	12.0	4.8	8
28	HN	26	HN	7.1	6.2	8
28	HN	30	HN	7.8	6.6	8
29	HN	11	HB#	12.0	2.3	8
29	HN	25	HN	12.0	8.1	8
29	HN	30	HD1#	6.0	5.1	8
31	HN	8	HN	12.0	7.2	8
32	HN	8	HN	12.0	7.8	8
32	HG2#	32	HN	3.2	3.7	8
32	HN	47	HD21	12.0	8.1	8
33	HD1#	8	HN	12.0	6.9	8
33	HN	9	HG1#	12.0	4.0	8
33	HD2#	34	HN	4.6	4.6	8
33	HN	35	HN	6.6	6.3	8
33	HN	44	HN	12.0	7.9	8
34	HN	35	HN	2.9	2.2	8
34	HD2#	43	HN	12.0	6.8	8
34	HN	44	HG2#	12.0	5.1	8
34	HN	49	HN	12.0	11.1	8
35	HN	32	HN	9.7	8.7	8
35	HN	33	HD2#	5.9	4.6	8
38	HD21	41	HE1	11.8	7.9	8
40	HN	41	HE1	9.7	6.3	8
41	HN	41	HE1	7.5	5.6	8
41	HN	43	HN	7.5	6.7	8
41	HN	53	HN	12.0	6.9	8
41	HE1	55	HN	12.0	6.5	8
42	HE1	33	HD1#	12.0	5.2	8
42	HE1	35	HD21	12.0	10.1	8
42	HE1	43	HN	7.8	6.5	8
42	HN	44	HG2#	7.6	5.4	8
42	HN	53	HG1#	12.0	5.3	8
42	HE1	56	HN	12.0	7.0	8
42	HN	56	HN	12.0	6.0	8
43	HN	33	HD2#	12.0	5.9	8
44	HG2#	43	HN	5.5	5.3	8
44	HN	44	HG2#	3.3	2.3	8
44	HN	53	HG1#	12.0	4.4	8
45	HN	35	HN	12.0	6.4	8
45	HN	50	HE22	12.0	7.1	8
45	HN	52	HN	12.0	8.9	8
46	HN	23	HN	12.0	8.0	8
47	HD21	47	HD22	1.7	1.7	8
49	HN	47	HD21	9.4	6.1	8
50	HN	50	HE21	7.0	5.6	8
51	HN	23	HG2#	12.0	4.0	8
51	HN	24	HN	12.0	7.3	8
51	HN	50	HE22	7.9	7.3	8

51	HN	53	HG2#	7.3	6.0	8
52	HN	19	HN	12.0	7.2	8
52	HN	23	HG1#	12.0	3.6	8
52	HN	24	HN	12.0	7.3	8
52	HN	50	HN	7.8	7.4	8
53	HN	22	HN	12.0	8.0	8
53	HG2#	23	HN	12.0	5.2	8
53	HG2#	42	HE1	12.0	7.3	8
53	HN	42	HE1	12.0	8.6	8
53	HG2#	43	HN	12.0	5.4	8
53	HG1#	52	HN	5.8	4.6	8
53	HN	53	HG2#	3.3	2.3	8
55	HN	25	HE#	12.0	6.5	8
55	HB#	42	HE1	12.0	3.0	8
55	HB#	56	HN	2.6	2.6	8
56	HN	53	HN	9.1	8.0	8
56	HN	56	HB#	2.0	2.2	8
56	HB#	57	HN	2.8	3.0	8
56	HN	58	HG2#	7.1	4.9	8
56	HN	59	HN	10.2	8.7	8
57	HN	53	HN	9.1	7.6	8
57	HN	58	HG2#	5.7	3.9	8
57	HN	59	HN	7.9	6.9	8
58	HN	9	HN	12.0	9.4	8
58	HG1#	11	HN	12.0	4.3	8
58	HN	12	HD1#	12.0	3.7	8
58	HN	42	HE1	12.0	8.5	8
58	HG1#	58	HN	3.3	3.0	8
58	HN	58	HG2#	3.3	2.4	8
58	HG2#	59	HN	3.6	3.3	8
58	HN	60	HN	7.5	6.3	8
59	HN	9	HG2#	12.0	4.0	8
59	HN	11	HB#	12.0	5.4	8
61	HN	9	HG1#	12.0	3.5	8
61	HN	31	HN	12.0	7.3	8

Supplementary Table 3: Torsion angle restraints obtained from TALOS+[8].

Residue	Phi	Phi error	Psi	Psi error
6	-124	35	157	25
7	-140	52	154	43
8	-119	47	147	26
9	-138	21	160	15
10	-118	27	123	18
11	-81	12	123	23
12	-95	14	-44	10

13	-144	59	162	17
16	-121	34	124	21
17	-94	40	134	46
23	-146	36	158	26
24	-119	33	141	32
25	-128	39	132	23
26	-121	55	139	51
27	-62	29	130	16
30	-97	37	116	42
31	-93	27	129	20
32	-98	21	125	24
34	-96	33	-36	25
38	-99	69	150	44
39	-65	31	-30	17
40	-99	32	-16	30
41	-133	29	135	37
42	-123	27	137	41
43	-110	33	131	24
44	-131	16	158	18
45	-130	29	135	23
46	-102	54	133	30
50	-128	47	154	26
52	-112	50	152	32
55	-57	13	-35	12
56	-68	15	-14	14
58	-130	33	158	24
59	-124	42	132	26
61	-106	63	109	37

References:

(1) Linser, R.; Fink, U.; Reif, B. *J. Am. Chem. Soc.* **2010,** *132*, 8891-8893.
(2) Lesage, A.; Gardiennet, C.; Loquet, A.; Verel, R.; Pintuacuda, G.; Emsley, L.; Meier, B. H.; Böckmann, A. *Angew. Chem. Int. Ed.* **2008,** *47*, 5851-5854.
(3) Linser, R.; Fink, U.; Reif, B. *J. Am. Chem. Soc.* **2009,** *131*, 13703-13708.
(4) Zhou, D. H.; Shea, J. J.; Nieuwkoop, A. J.; Franks, W. T.; Wylie, B. J.; Mullen, C.; D. Sandoz; Rienstra, C. M. *Angew. Chem. Int. Ed.* **2007,** *46*, 8380-8383.
(5) Brünger, A. T.; Adams, P. D.; Clore, G. M.; DeLano, W. L.; Gros, P.; Grosse-Kunstleve, R. W.; Jiang, J. S.; Kuszewski, J. J.; Nilges, M.; Pannu, N. S.; Read, R. J.; Rice, L. M.; Simonson, T.; Warren, G. L. *Acta Crystallogr. D Biol. Crystallogr.* **1998,** *54*, 905-921.
(6) Nilges, M.; O'Donoghue, S. I. *Prog. Nucl. Mag. Res. Sp.* **1998,** *32*, 107-139.
(7) Linge, J. P.; Nilges, M. *J. Biomol. NMR* **1999,** *13*, 52-59.
(8) Shen, Y.; Delaglio, F.; Cornilescu, G.; Bax, A. *J. Biomol. NMR* **2009,** *44*, 213-23.